Contents

7.1. INTRODUCTION

For potent drugs like VPN and NPT, it is important to have a delivery system capable of delivering calculated dose in error-free manner. Fast dissolving microneedles were chosen to incorporate optimized nanocarriers owing to the advantage of physically breaching stratum corneum barrier and rapidly releasing the cargo in deeper skin layers. Fast dissolving microneedles also avoid the risk of cross-

contamination and accidental breakage associated with metal or other non-biodegradable microneedles [1].

A simplified micromold casting method was used for fabrication of fast dissolving microneedle patches that requires less production time and cost and holds promise for large scale production [2]. A systematic Quality-by-design (QbD) approach employing statistical design of experiments was utilized to exhaustively evaluate the impact of material attributes and process parameters on the critical formulation attributes [3].

7.2. MATERIALS & METHODS

7.2.1 Materials

DermaStamp L4001 (35 titanium microneedles) were purchased from Guangzhou Junguan Beauty Co. Ltd., China. Poly-dimethylsiloxane (Sylgard® 184) was purchased from Dow corning, United States. Poly vinyl alcohol (MW, 6 kD) and Poly vinyl pyrollidone (MW, 3.5 kD) were purchased from Acros organics, Mumbai, India. Transdermal patch components, viz., high adhesion double coated medical tape (1567), Scotchpak™ 9735 backing film and Scotchpak™ 9741 release liner, were obtained as a generous gift from 3M™, USA. Double distilled water was prepared in lab, filtered through 0.2μ membrane filter in glass bottle and consumed within a maximum of 7 days.

7.2.2 Preparation of poly-dimethylsiloxane (PDMS) micromolds

Micromolds of poly-dimethylsiloxane (PDMS) were prepared using 35 titanium microneedles dermastamp (L4001) as master templates. Briefly, silicone elastomer and curing agent were mixed in a weight ratio of 10:1 and taken in suitable molding containers. The master templates were carefully inserted into the containers avoiding any air bubble and kept overnight at room temperature for partial curing. After 12 hours, master templates were removed and the micromolds were completely cured at 90°C for 8 hours in a waterbath. The micromolds were separated from containers and used for fabrication of fast dissolving microneedle patch.

7.2.3 Preparation of fast dissolving microneedle patch

Low molecular weight poly vinyl alcohol (PVA) and poly vinyl pyrollidone (PVP) were used as binder and filler, respectively for the preparation of microneedle matrix. Different amounts of PVA was dissolved in distilled water by gentle stirring at 80 °C using a hot plate magnetic stirrer and later cooled to room temperature. Varying amounts of PVP was then added and dissolved by stirring at room temperature. The resulting PVA/PVP blend solutions were transferred to PDMS micromolds. The filling of microneedle cavities of these micromolds was facilitated by centrifugation at 3000 rpm and 25 °C for 10 minutes. These micromolds were then kept in vacuum desiccators for 24 hours for evaporation of water and hardening of the microneedle structure. The resulting microneedle arrays were carefully removed from the micromolds using 1567 high adhesion double coated medical tape (3M™, USA) with backing film on other adhesive side. Release liner was then placed to cover remaining adhesive layer while avoiding contact with microneedles. Resulting MNP were stored in an airtight container with silica gel and calcium oxide as desiccants.

7.2.3.1 Establishing Quality target product profile and Critical Quality Attributes

Based on the scientific, therapeutic, industrial and regulatory aspects, quality target product profile (QTPP) for fast dissolving microneedle patches were established. Further, based on the prior knowledge, literature review and experiment trials, axial needle fracture force (ANFF) was selected as critical quality attribute (CQA).

7.2.3.2 Identification of Independent variables (factors) and qualitative risk assessment

Ishikawa diagram was used to demonstrate all the probable variables associated with the fabrication of fast dissolving microneedles by micromold casting method. These factors were qualitatively categorized as 'low, medium and high risk' based on their impact on CQA as described in **Table 7-1**.

Table 7-1. Quality risk assessment criteria

Low Risk	Factors with wide range of acceptability. No investigation required
Medium Risk	Acceptable risk. No adverse effect on product quality on small changes.
High Risk	Unacceptable risk. Acceptable range need to be investigated

Factors with low and medium risk were controlled by assigning constant levels based on literatures and preliminary trials.

7.2.3.3 Formulation optimization by combined D-optimal response surface design

Combined D-optimal response surface design was applied to exhaustively investigate the relationship between High risk (critical) factors and CQA with less number of experimental batches while handling mixture components and other numeric factors simultaneously [4]. Design Expert® 7.0.0 was used for generating the randomized design matrix and statistical evaluation of experimental data to achieve optimization solution and creating the design space. Suitability of model suggested by the software and identification of significant model terms were decided based on analysis of variance followed by F-test. Insignificant model terms were later removed to simplify the mathematical equations for calculation of CQA. The relationship between critical factors and CQA was explored using contour and 3-D response surface plots. Desirability criteria was defined based on QTPP and design space was created to obtain final optimized batch. Three batches were prepared with optimized composition for model verification. Method used for estimation of CQA is as follows.

7.2.3.3.1 Axial needle fracture force measurement

Axial needle facture force was measured using CT3 texture analyzer (Brookfield, UK). The microneedle arrays were mounted on the moving probe of the instrument using double sided adhesive tapes in such ways, so as to keep the axis of microneedles parallel to the axis of moving probe. The probe was then programmed to press the microneedles against a flat, rigid stainless steel block [5]. The needle strength was then

evaluated utilizing the load versus distance graphs generated by TexturePro CT data acquisition software.

7.2.4 *In vitro* characterization of fast dissolving MNP

7.2.4.1 Shape and surface morphology

For characterization of microneedles shape and their surface morphology, fast dissolving MNP were affixed on sample stub and observed under JSM-5610LV scanning electron microscope (JEOL, Japan) at an accelerating voltage of 20 kV.

7.2.4.2 Skin penetrability

The microneedle arrays were mounted on the moving probe of CT3 texture analyzer (Brookfield, UK) using double sided adhesive tapes in such ways, so as to keep the axis of microneedles parallel to the axis of moving probe. The probe was then programmed to press the microneedles against full thickness pig ear skin affixed, under a mild tension, on to soft sponge pad [6], to simulate *in situ* mechanical support, at an insertion speed of 20 mm/s [7]. The microneedle treated skin area was exposed to trypan blue dye for 5 minutes. Excess dye was cleaned using phosphate buffer saline (pH 7.4) and the images of stained pores were captured using digital camera.

7.2.4.3 Pore closure study

Full thickness pig ear skin was affixed, under a mild tension, on to soft sponge pad to simulate *in situ* mechanical support. Fast dissolving MNP was then applied for different time periods up to 24 hours. At each time points, MNP was removed and sections of epidermis were taken using cryo-microtome to observe for pore formation under Eclipse H600L inverted microscope (Nikon, Japan).

7.2.5 Preparation of nanocarriers loaded fast dissolving MNP

Aqueous dispersion of optimized VPN and NPT loaded UDL and PNP were taken in round bottom flasks and the water was evaporated to 1/10th of the initial formulation weight using a rotary vacuum evaporator at 500 mm of Hg negative pressure. Concurrently, polymer blend solutions with optimized ratio of PVA-to-PVP were prepared in similar

way as described earlier in this chapter. The concentrated formulations were then added to the polymer blend solutions to get the final solid content of mixture at optimized level (Table 7-13). Resulting solutions were filled in micromolds and fast dissolving MNP were fabricated using the method described earlier in this chapter. These MNP were stored in an airtight container with silica gel and calcium oxide as desiccants.

7.2.6 *In vitro* characterization of nanocarriers loaded fast dissolving MNP

7.2.6.1 Shape and surface morphology

All four nanocarriers loaded fast dissolving MNP were observed under Eclipse H600L inverted microscope (Nikon, Japan) for shape and morphological characteristics.

7.2.6.2 Axial needle fracture force measurement

Similar method was used for axial needle fracture force measurement as described in section 7.2.3.3.1.

7.2.6.3 In vitro dissolution time

Full thickness pig ear skin was affixed, under a mild tension, on to soft sponge pad impregnated with phosphate buffer 6.8 for skin equilibration. Nanocarriers loaded fast dissolving MNP were then applied for different time periods up to 120 seconds, removed and observed under Eclipse H600L inverted microscope (Nikon, Japan) for changes in microneedle length as a measure of its dissolution.

7.2.6.4 Physical stability of nanocarriers in fast dissolving MNP

Physical stability of nanocarriers in fast dissolving MNP was evaluated immediately after its preparation. The MNP were dissolved in prefiltered distilled water and the resulting dispersion of nanocarriers were evaluated for their shape, size and entrapment efficiency using the methods described in previous chapters.

7.2.6.5 In vitro drug release

The *in-vitro* drug release from nanocarriers loaded fast dissolving MNP were evaluated using a Franz-type diffusion cell with a receptor chamber volume of 15 ml. Pre-activated dialysis membrane (MWCO, 12

kD) was mounted, as a permeation barrier, between donor and receptor chambers of diffusion cell. The receptor chamber was filled with a mixture of ethanol and double distilled water (ratio 3:7) as a diffusion media and allowed to equilibrate for half an hour. The MNP were dissolved in prefiltered distilled water and equivalent amount of resulting dispersions containing 1 mg of drug were transferred to donor chambers of diffusion cells. The diffusion medium was continuously stirred using a magnetic stirrer. 1 mL sample was withdrawn from sampling arm of diffusion cell at each time point up to 24 hours and equal volume of fresh diffusion media was added to maintain total receptor volume. Quantitative estimation of VPN and NPT was done using the methods described in previous chapters. The kinetics of drug release was then evaluated by fitting the data in various mathematical models and comparing their regression coefficient (R^2) values [8].

7.3. RESULTS & DISCUSSION

7.3.1 Preparation of PDMS micromolds

The process of micromold formation and characterization is illustrated in **Fig. 7-1**.

PDMS micromold were prepared exactly complimentary to master structure. Microscopic evaluation of micromolds showed smooth and conical microneedle cavities.

7.3.2 Preparation and optimization of fast dissolving MNP

7.3.2.1 Establishing QTPP and CQA

Various QTPP elements and their targets were defined and presented with justification in **Table 7-2**.

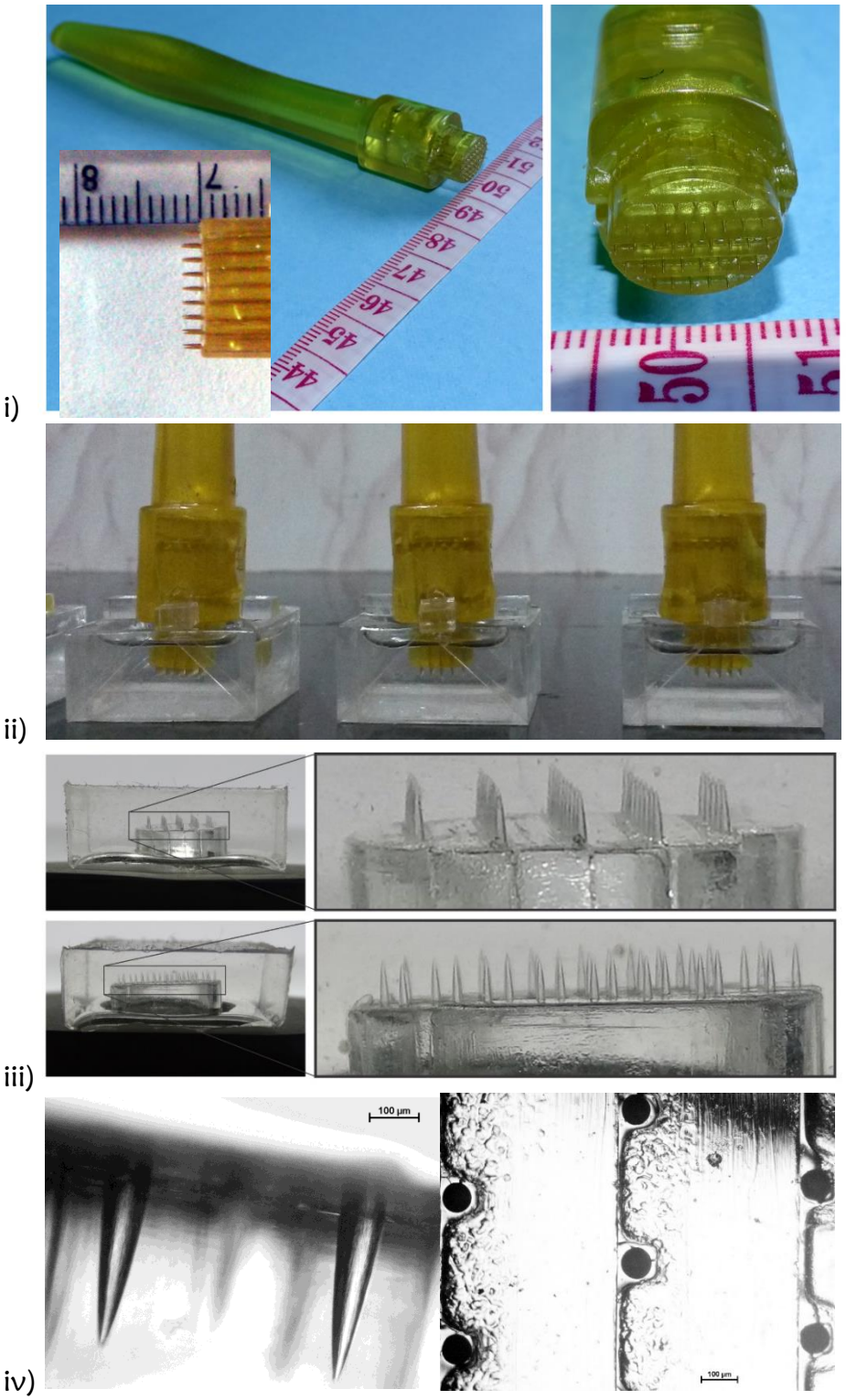

Fig. 7-1. i) Dermastamp L4001 with 36 titanium microneedles of 1.5 mm length; ii) Dermastamp dipped in PDMS to create micromolds; iii) Photograph of PDMS micromold; iv) Microscopic images of PDMS micromold showing microneedle cavities (front and top view).

Table 7-2. QTPP elements with justification for fast dissolving MNP

QTPP element		Target	Justification
Route of administration		Transdermal	Avoid first pass metabolism and achieve prolonged action
Dosage form		Microneedle Patch	Ability to breach stratum corneum barrier and augment permeation of payload
Formulation quality attributes	Needle length	NMT 1.5 mm	To ensure skin piercing in painless manner
	Axial needle fracture force[#]	Maximize (> 0.6N)	To ensure penetration of intact needles without breaking.
	Skin penetrability	Yes	To ensure skin breaching by microneedles
	Surface characteristics	Smooth	To ensure easy penetration
	In vitro dissolution	Within 5 minutes	To ensure fast release of drug loaded nanocarriers
Safety		Non-toxic & Non-irritant to skin	To ensure safety of the final formulation

[#] Critical quality attributes

Axial needle fracture force (ANFF) was identified as critical in governing the product quality and need to be within known limits to attain the pre-defined QTPP. Thus, ANFF was selected as CQA.

7.3.2.2 Identification and qualitative assessment of Independent variables (factors)

All the probable variables associated with development of fast dissolving MNP by micromold casting method were identified during the brainstorming sessions and categorized in to Material, Process, Equipment, Personnel and Environment. An ishikawa diagram illustrating the cause and effect relationship among identified variables and CQA was constructed (**Fig. 7-2**).

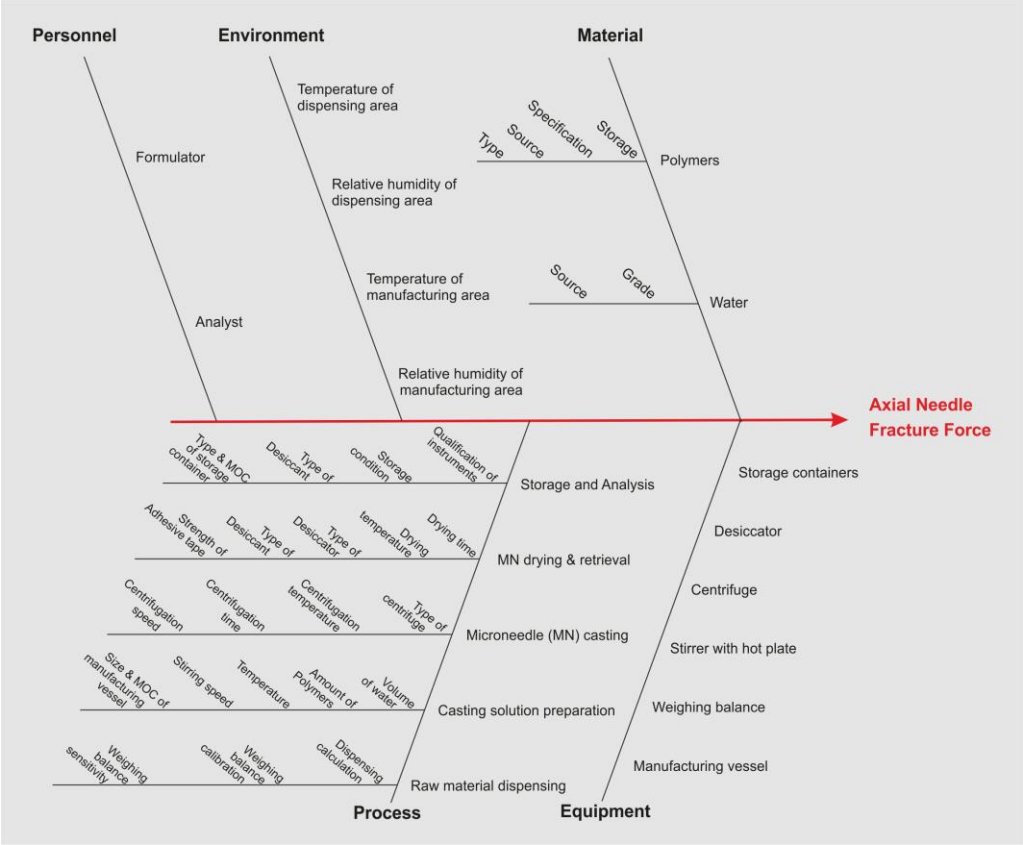

Fig. 7-2. Ishikawa diagram showing probable variables that may influence the CQA

7.3.2.3 Qualitative risk assessment

The risk associated with all the identified factors were evaluated based on the predefined criteria (**Table 7-1**) and the result is presented in **Table 7-3** Factors with low and medium risk were assigned with the best available constant levels based on literature and preliminary trials to ensure no or negligible impact of these factors on CQA. These constant levels are also listed in **Table 7-3**.

Table 7-3. Qualitative risk assessment of independent variables

Factors	Process step	Impact on CQA	Constant levels
Polymer as binder to provide needle strength	Raw material Selection and Storage	Low risk	Low MW polyvinyl alcohol (PVA)
Polymer as filler to augment dissolution		Low risk	Low MW polyvinyl pyrrolidone (PVP)
Source and specifications of Polymers		Low risk	Authentic source with COA
Storage condition of Polymers		Low risk	Stored at recommended condition
Source of water		Low risk	In house

Factors	Process step	Impact on CQA	Constant levels
Grade of water		Low risk	Filtered (0.2µ) Double distilled
Weighing balance sensitivity	Dispensing	Low risk	0.1 mg
Weighing balance calibration		Low risk	Calibrated
Temperature and RH of Dispensing Area		Low risk	25±3°C, Ambient RH
Dispensing calculations		Low risk	Calculated using excel and verified
Type, Size and Material of Construction (MOC)	Manufacturing Vessel	Low risk	20 mL bottle of class A borosilicate glass
Temperature and Relative humidity	Manufacturing Area	Low risk	25±3°C, Ambient RH
Volume of Water	Preparation of Casting solution	High risk	To be optimized
Amount of PVA		High risk	To be optimized
Amount of PVP		High risk	To be optimized
Stirring speed of Aqueous phase		Low risk	500 rpm
Temperature of Aqueous phase		Low risk	90°C– PVA dissolution 25°C– PVP dissolution
Type of Centrifuge	Microneedle fabrication	Medium risk	Centrifuge with swing bucket rotor head
Centrifugation speed		Medium risk	3000 rpm
Centrifugation time		Low risk	30 min
Centrifugation temperature		Low risk	25 °C
Drying time	Drying of Microneedles	Low risk	24 hours
Drying temperature		Low risk	Room Temperature
Type of dryer		Low risk	Desiccator with vacuum and silica gel and calcium oxide as desiccants
Adhesive tape	Microneedle removal and patch formation	Low risk	high adhesion double coated medical tape (1567), 3M
Release Liner		Low risk	Scotchpak™ 9741 release liner, 3M
Backing membrane		Low risk	Scotchpak™ 9735 backing film, 3M
Storage condition	Storage and Analysis	Low risk	In Desiccator at RT with silica gel and calcium oxide as desiccants
Calibration of Analytical Instruments		Low risk	Calibrated
Formulator	Personnel	Low risk	Common for all experiments and analysis
Analyst		Low risk	

Three factors were identified to have high risk and were carried forward for formulation optimization.

7.3.2.4 Formulation optimization by combined D-optimal response surface design

Based on qualitative risk assessment, three CMA were identified and their relationship with CQA were exhaustively investigated using combined D-optimal response surface design. Combined D-optimal design was selected as it allowed the evaluation of PVA to PVP ratio in polymer blend together with numerical variable viz., total solid content. The low (-1), medium (0) and high (+1) levels of all three CMA are listed in **Table 7-4**. Amount of PVA and PVP in polymer blend was varied in such a way to keep the total as 100%.

Table 7-4. Various critical material attributes along with their levels for optimization by Combined D-optimal design

Independent variables (CMA)		Unit	Levels		
			-1	0	+1
A:	PVA in polymer blend	%	70	80	90
B:	PVP in polymer blend	%	10	20	30
C:	Total solid content	% w/w	35	40	45

A randomized matrix of nineteen batches was generated by Design-Expert and presented in **Table 7-5**. These batches were formulated as per their run order and evaluated for CQA using the methods described earlier. **Table 7-5** also represents the resulting CQA of these batches.

Table 7-5. Randomized design matrix for Combined D-optimal response surface design

Batch no.	Run order	Independent Variables			CQA
		A	B	C	Axial needle fracture force (N)
F_1	9	80	20	40	0.506
F_2	17	90	10	40	0.708
F_3	2	80	20	35	0.466
F_4	8	80	20	45	0.516
F_5	15	70	30	35	0.154
F_6	3	70	30	45	0.151
F_7	4	70	30	40	0.172
F_8	18	90	10	35	0.691
F_9	10	90	10	45	0.702
F_{10}	6	75	25	37.5	0.347
F_{11}	11	75	25	42.5	0.324

Batch no.	Run order	Independent Variables			CQA
		A	B	C	Axial needle fracture force (N)
F_{12}	5	85	15	37.5	0.591
F_{13}	19	85	15	42.5	0.618
F_{14}	14	70	30	37.5	0.166
F_{15}	1	90	10	45	0.706
F_{16}	7	90	10	35	0.685
F_{17}	13	70	30	45	0.177
F_{18}	16	70	30	35	0.170
F_{19}	12	80	20	45	0.506

Based on the experimental data of axial needle fracture force (ANFF), software suggested quadratic model for mix order and linear model for process order. Analysis of variance (ANOVA) was performed by the software for suggested models. Model terms with a p-value less than or equal to 0.05 (α-level) were considered as significant while terms with higher p-value were considered insignificant. Considering the hierarchy, no insignificant model terms were removed by the software during model reduction. Hence, full model was utilized to obtain optimization solution.

ANOVA and coded coefficients of Full model for ANFF are presented in **Table 7-6** and **Table 7-7**, respectively.

Table 7-6. Analysis of variance of full quadratic model for axial needle fracture force

Source	Full model				
	DF	Adj SS	Adj MS	F-Value	P-Value
Model	5	0.8785	0.1757	1246.45	< 0.0001
Linear Mixture	1	0.8629	0.8629	6121.73	< 0.0001
AB	1	0.0122	0.0122	86.56	< 0.0001
AC	1	0.0003	0.0003	2.34	0.1500
BC	1	4.00321E-06	4.00321E-06	0.03	0.8688
ABC	1	0.0005	0.0005	3.60	0.0801
Residual	13	0.0018	0.0001	-	-
Lack-of-Fit	8	0.0013	0.0002	1.49	0.3436
Pure Error	5	0.0005	0.0001	-	-
Total	18	0.8803	-	-	-

As showed in ANOVA table, the linear mixture and interactive effects between PVA and PVP were found to affect ANFF significantly. An insignificant lack-of fit showed the adequacy of the model in explaining the variation in the responses.

Table 7-7. Coded coefficients of full quadratic model for axial needle fracture force

Term	Full Model		
	Coefficient	SE Coefficient	VIF
A-PVA	0.698	0.005	1.37
B-PVP	0.164	0.005	1.33
AB	0.235	0.025	1.76
AC	0.009	0.006	1.24
BC	-0.001	0.007	1.24
ABC	0.059	0.031	1.53

Coefficients table for ANFF showed VIF values near to 1 indicating that the predictors are not correlated and regression coefficients are well estimated. Regression equation for full model in uncoded units is presented as **Eq. 7-1**. The positive and negative sign before each coefficients indicates a direct or inverse relationship of that model term with ANFF.

$$R1 = 1.031A + 2.319B - 5.931AB - 0.006AC - 0.193BC + 0.295ABC$$

Eq. 6-1

Model summary for ANFF is presented in **Table 7-8**. A low SD value and high R^2 value indicated a better prediction of responses by the model. Predicted R^2 was found to be in good agreement with other R^2 further supporting the prediction potential of the model.

Table 7-8. Summary of full quadratic-linear model for ANFF

Responses	Full model			
	SD	R-sq	R-sq (adj)	R-sq (pred)
Axial needle fracture force (N)	0.0119	99.79	99.71	99.59

Four different residual plots viz., normal plot of residual, residual versus ascending predicted response values, residual versus experimental run order and predicted versus actual were generated for ANFF and presented in **Fig. 7-3**. In normal plot, residuals were appeared to follow a straight line indicating that the data was normally distributed. Random scattering without any megaphone pattern in residual versus predicted plot validated the assumption of constant variance. Similarly, random scattering without any pattern in residual versus run plot validated the absence of lurking variables. In predicted versus actual plot, data points

were evenly split by the 45 degree line indicating easy prediction of values by the model.

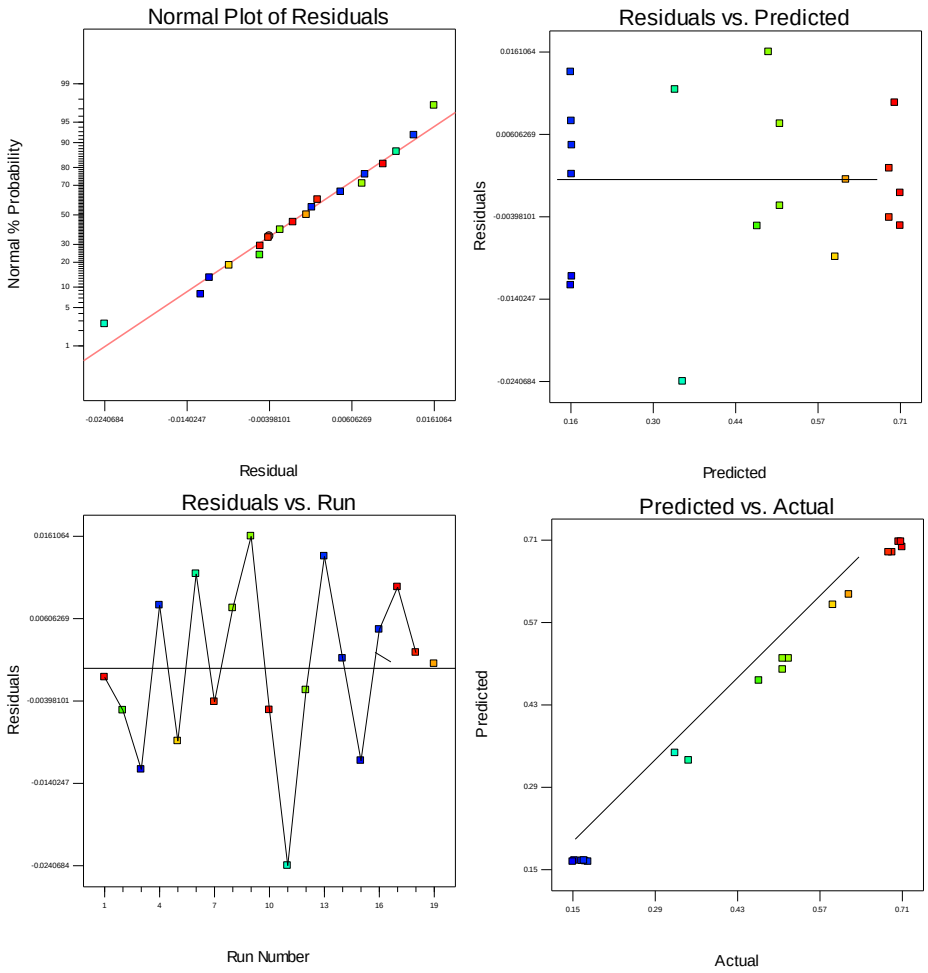

Fig. 7-3. Residual plots for axial needle fracture force

The main effect plots for ANFF are presented in **Fig. 7-4**.

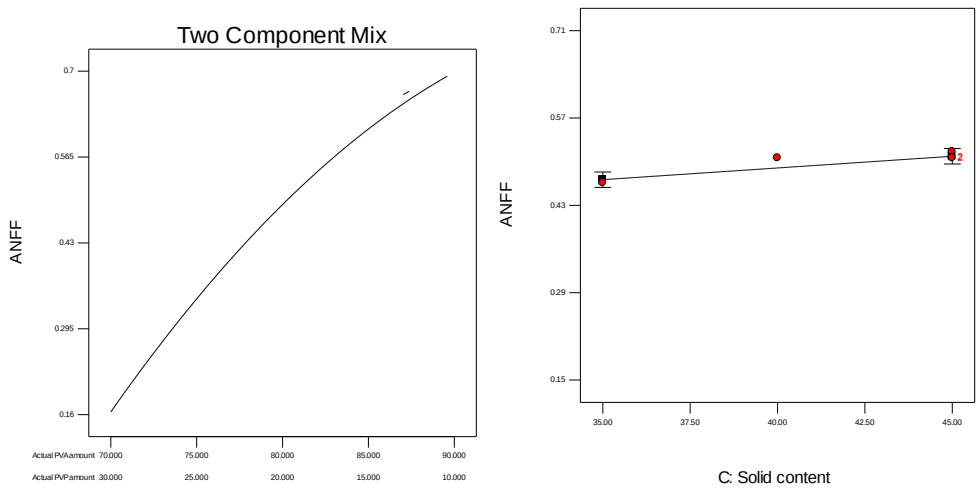

Fig. 7-4. Main effect plots for ANFF

These graphs provided a better depiction of how the individual CMA influence ANFF and found in-line with the ANOVA results.

Contour and response surface plots are presented in **Fig. 7-5**. This graph was used to depict how the ANFF is related to respective CMA.

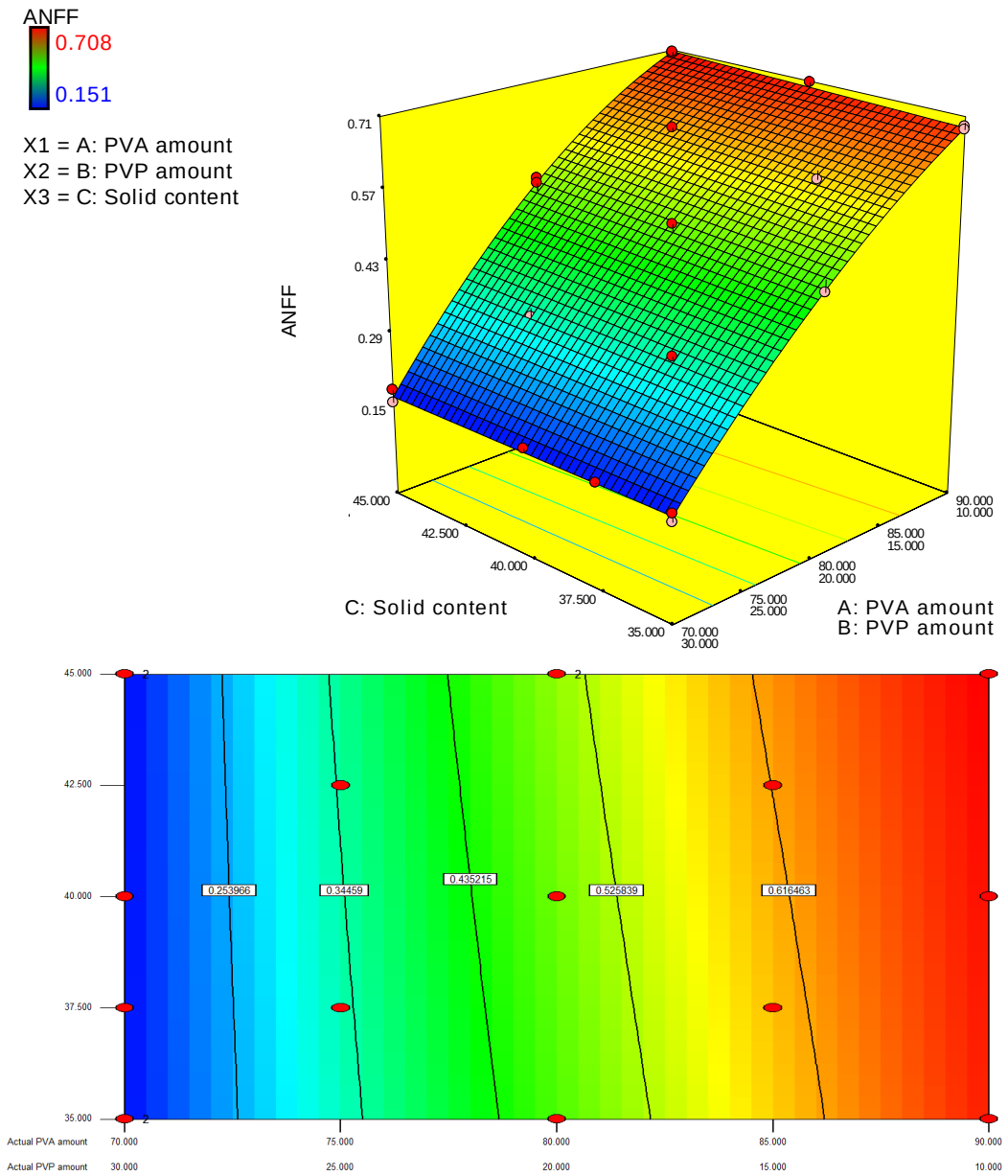

Fig. 7-5. Contour and response surface plots for axial needle fracture force

Numerical optimization was performed by the software for defined optimization criteria as presented in **Table 7-9**. The software was programmed to provide the optimization solution with Maximum ANFF while keeping all the CMA within experimental range.

Table 7-9. Criteria for optimization of fast dissolving MNP

Constraints name	Goal	Lower	Upper	Weight	Importance
PVA Amount	in range	70	90	1	3
PVP Amount	in range	10	30	1	3
Total solid content	in range	35	45	1	3
Axial needle fracture force	maximize	0.151	0.708	1	3

Further, the desirability plot is presented in **Fig. 7-6**.

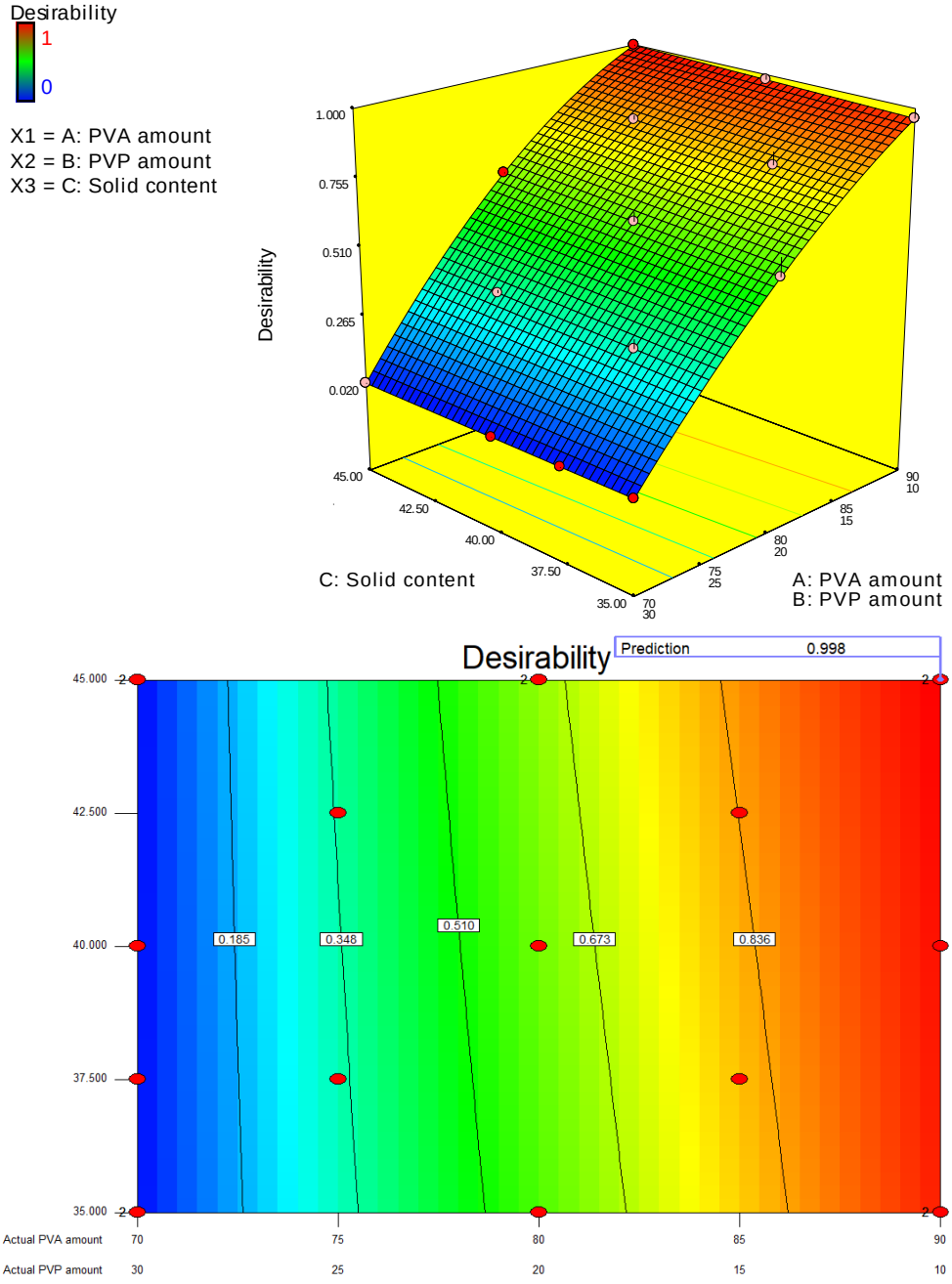

Fig. 7-6. A) Contour and B) Response surface plot of composite desirability for ANFF

The desirability plot showed a desirability of 0.998 for the solution provided by the software. The setting of this optimization solution is also presented in **Table 7-10** along with the 95% confidence as well as 95% prediction intervals. Three batches with optimized levels were prepared for verification trials and the values of ANFF are presented in **Table 7-11**.

Table 7-10. Optimization solution

Multiple Response Prediction

Variable	Setting
PVA (%)	90
PVP (%)	10
Total solid content (% w/w)	45

Responses	Fit	SE Fit	95% Confidence interval		95% Prediction interval	
			Lower	Upper	Lower	Upper
Axial needle fracture force (N)	0.707	0.008	0.690	0.724	0.676	0.738

Table 7-11. Results of verification trials

Responses	95% Prediction interval		Results			
	Lower	Upper	Batch-1	Batch-2	Batch-3	Average
Axial needle fracture force (N)	0.676	0.738	0.695	0.701	0.699	**0.698**

The average values of ANFF was found to fall within 95% confidence interval and thus indicated the validity of the model.

7.3.3 *In vitro* characterization of fast dissolving MNP

Photographs of optimized fast dissolving microneedle and its patch is shown in **Fig. 7-7**.

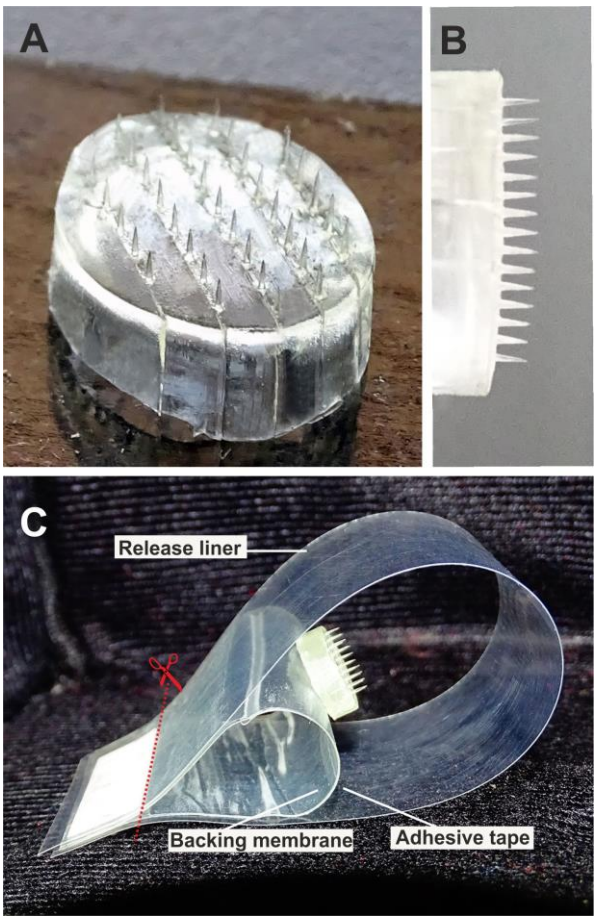

Fig. 7-7. Photograph of Microneedles A) top, B) side view and C) its patch.

The folded patch was designed to avoid microneedle damage by patch components. For application, the patch needs to be cut along the red dotted line followed by removal of release liner.

7.3.3.1 Shape and surface morphology of MNP

SEM images of fast dissolving MNP are presented in **Fig. 7-8**.

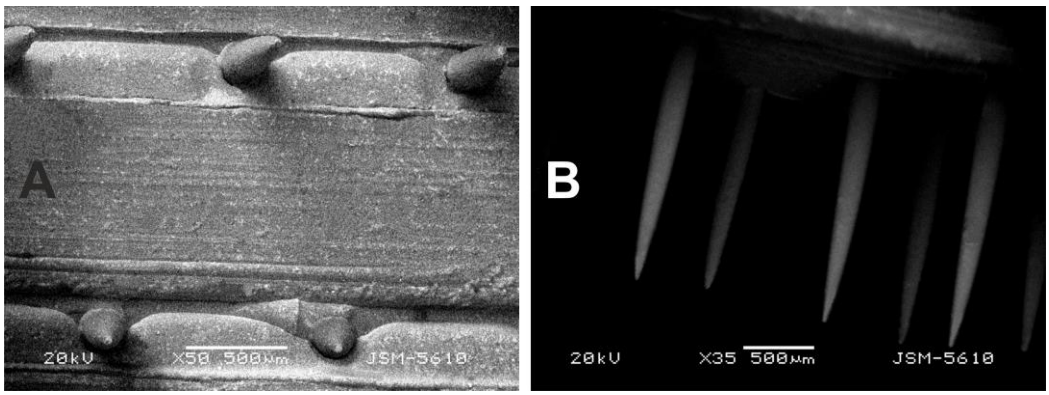

Fig. 7-8. SEM images of fast dissolving Microneedles A) top & B) side view

These images showed smooth surfaced, conical microneedles with 1.5 mm length, around 200 μm base diameter. The microneedle array

geometry observed in SEM images was suitable for skin piercing with minimal damage as available in literature [9].

7.3.3.2 Skin penetrability

The image of trypan blue stained skin section is presented in **Fig 7-9**. Presence of 35 stained pores clearly indicated that all 35 microneedles of MNP were able to penetrate the skin. A load versus time curve was also presented in **Fig 7-9** showing the axial needle fracture force of these MNP as 0.695 N. It can be thus stated that the MNP with an axial needle fracture force of around 0.7 N possess sufficient strength to breach stratum corneum barrier and to create microchannels for improved transdermal permeation.

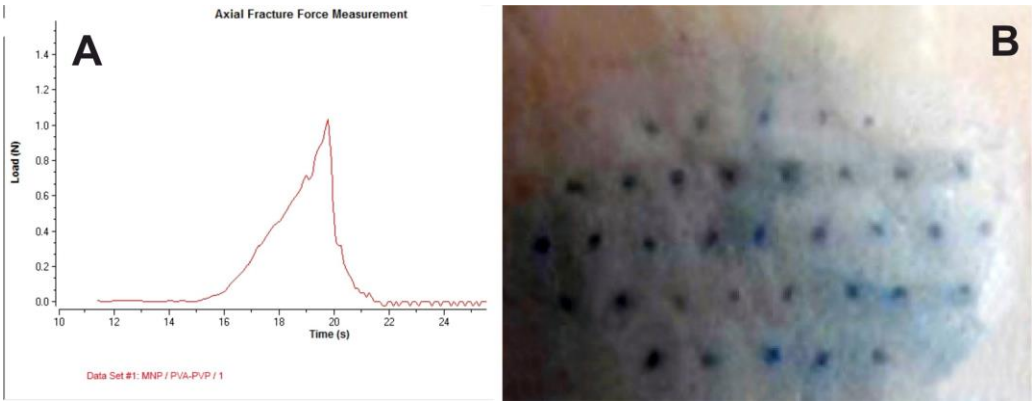

Fig. 7-9. A) Load versus time graph for ANFF measurement; B) Trypan blue stained pores on MNP treated pig ear skin

7.3.3.3 Pore closure study

The pores created in skin were observed under microscope and their average diameter were recorded. **Table 7-12** summarizes the data obtained for different time points while **Fig. 7-10** shows their representative images at 4X and 10X magnifications.

Table 7-12. Pore closure data at different time points

Time (h)	Average pore diameter (µm)*
0	94.6 ± 6.9
3	82.1 ± 7.6
6	68.8 ± 6.9
12	61.7 ± 5.2
18	54.5 ± 5.7
24	47.9 ± 6.1

* Values presented as mean ± SD

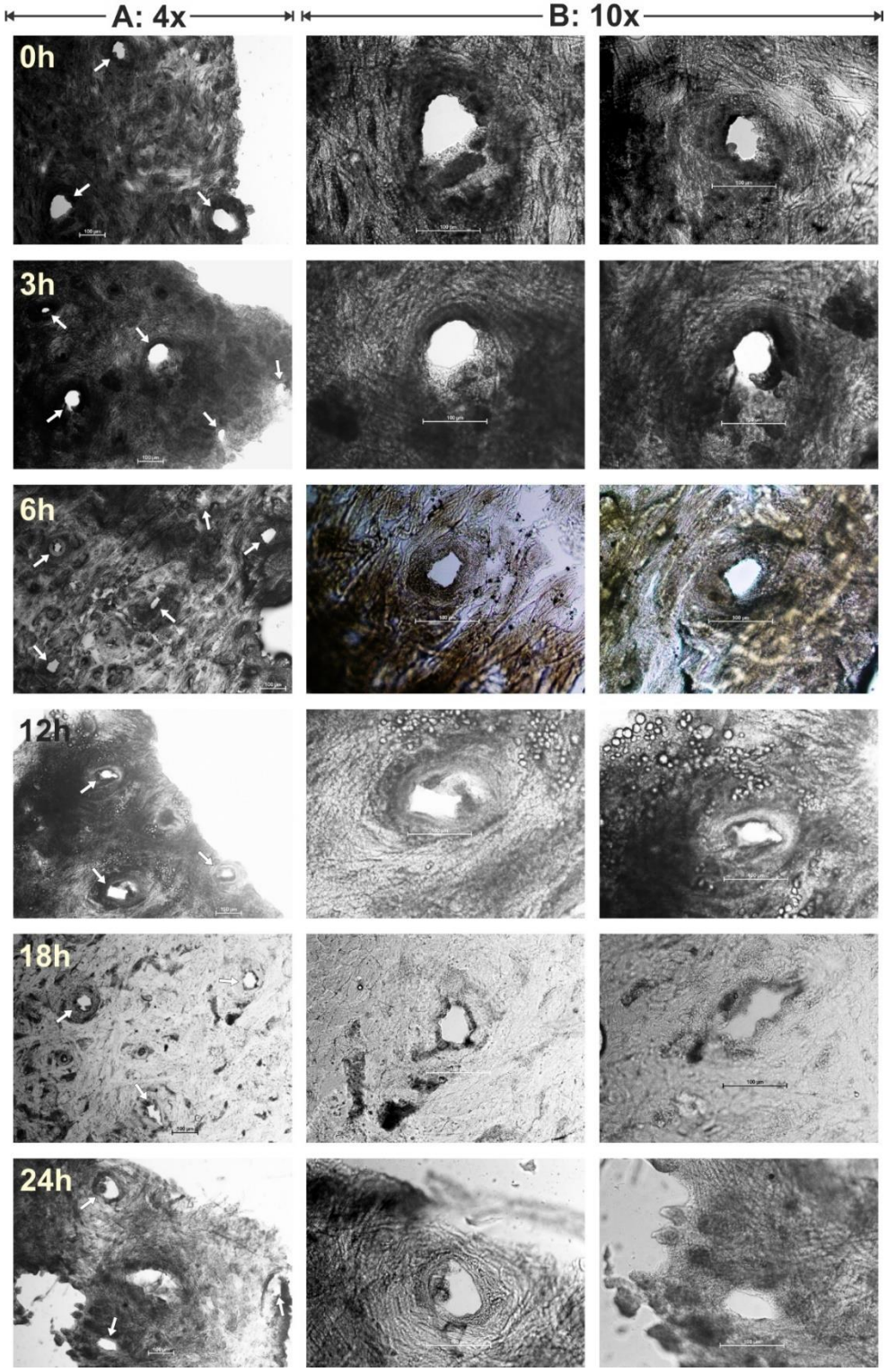

Fig. 7-10. Pig ear skin sections showing open pores till 24 hours under occlusive condition A) at 4X and B) at 10X magnification

It can be observed in **Fig. 7-10** that the pores created by fast dissolving MNP were remained open for 24 hours under occlusive conditions.

7.3.4 Preparation of nanocarriers loaded fast dissolving MNP

From the optimized composition of fast dissolving MNP, a fraction of PVA-PVP blend was replaced with the optimized liposomal or nanoparticulate formulations of VPN and NPT in such a way to keep the total solid content levels constant (Table 7-13).

Table 7-13. Total solid content calculation for nanocarriers loaded MNP

Formulations	Solid content of formulation (mg/0.5 g)	PVA and PVP in polymer blend (mg/1.5 g)		Total solid content (%w/w) of Polymer and formulation mix
		PVA	PVP	
VPN UDL	84.4	734.0	81.6	45
NPT UDL	84.3	734.1	81.6	45
VPN PNP	34.5	778.9	86.6	45
NPT PNP	34.5	778.9	86.6	45

7.3.5 *In vitro* characterization of nanocarriers loaded fast dissolving MNP

7.3.5.1 Shape and surface morphology of MNP

Optical microscopic images of VPN UDL MNP, VPN PNP MNP, NPT UDL MNP and NPT PNP MNP are presented in Fig. 7-11.

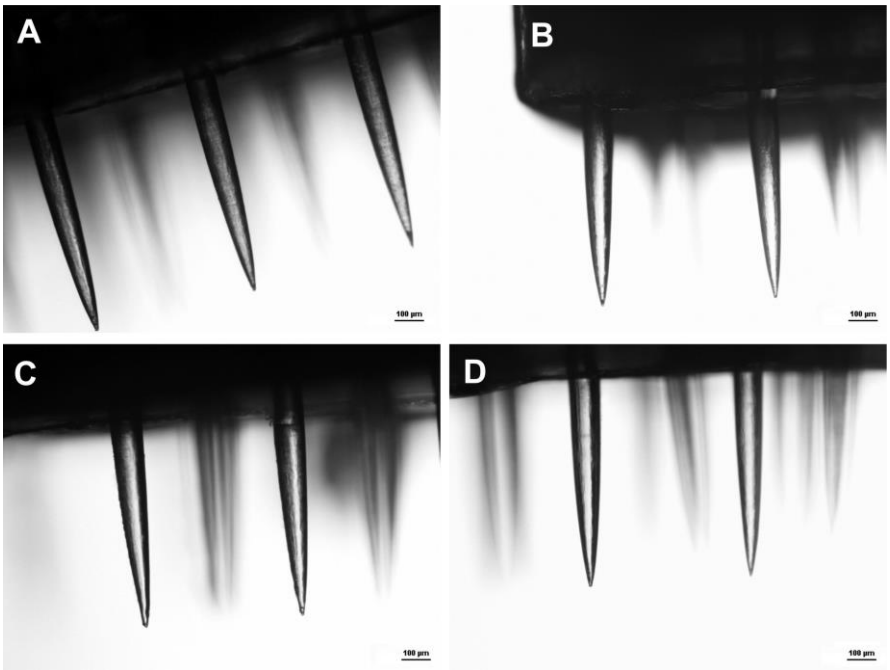

Fig. 7-11. Optical microscopic images of A) VPN UDL, B) VPN PNP, C) NPT UDL and D) NPT PNP loaded fast dissolving microneedles

A similar geometry was observed in all four formulation loaded fast dissolving MNP as compared to blank PVA-PVP MNP. This indicated successful incorporation of optimized nanocarriers in PVA-PVP

microneedle matrix. Smooth, conical microneedles can be clearly seen in the images.

7.3.5.2 Axial needle fracture force measurement

The strength of optimized nanocarriers loaded MNP were evaluated using axial needle fracture force measurement. The load versus time graphs are presented in **Fig. 7-12** and the data obtained are summarized in **Table 7-14**.

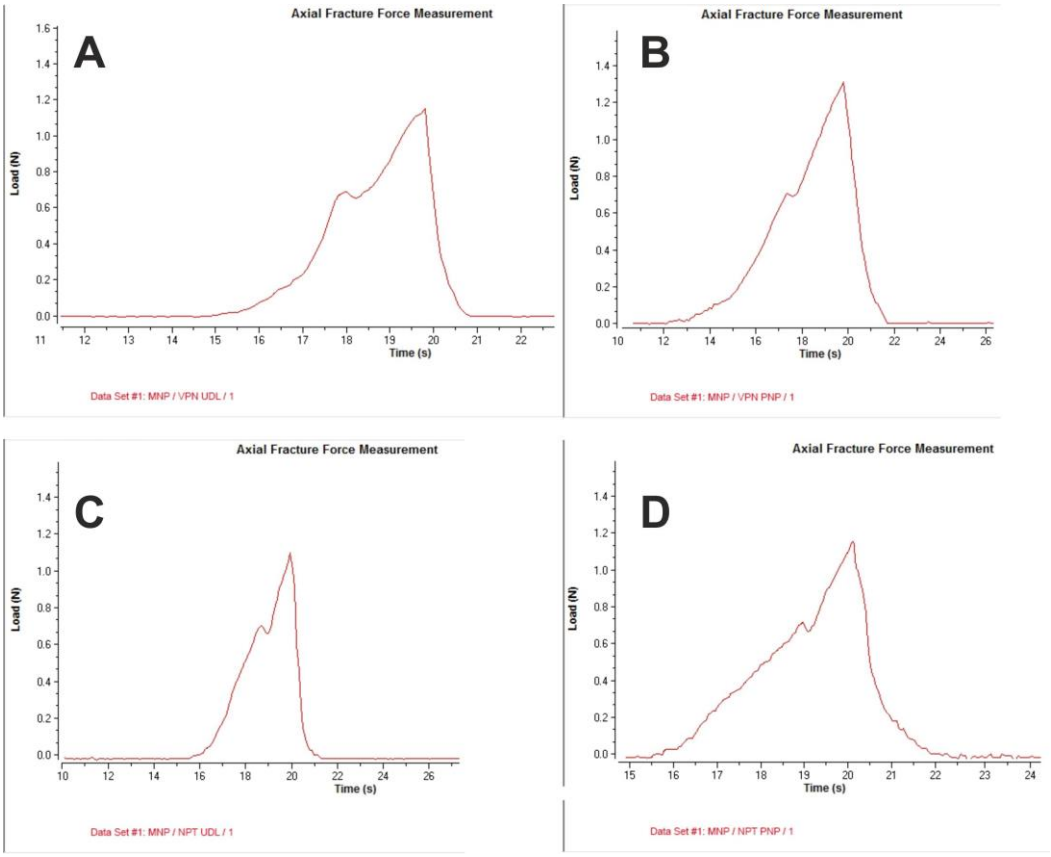

Fig. 7-12. Load versus time curve showing ANFF for microneedle patches of A) VPN UDL, B) VPN PNP, C) NPT UDL and D) NPT PNP.

Table 7-14. Axial needle fracture force of various nanocarriers loaded MNP

Formulations	Axial Needle Fracture Force (N)*
VPN UDL MNP	0.684 ± 0.04
NPT UDL MNP	0.688 ± 0.05
VPN PNP MNP	0.711 ± 0.05
NPT PNP MNP	0.704 ± 0.07

* Values represented as Mean ± SD (n=3)

The ANFF of nanoparticulate loaded MNP showed similar or better values as compared to blank PVA-PVP MNP, while liposomal nanocarriers loaded MNP showed insignificantly less ANFF values. Such

observations advocated that nanocarriers loaded MNP own almost similar strength as that of blank PVA-PVP MNP and thus should easily breach the skin surface as observed with blank PVA-PVP MNP.

7.3.5.3 In vitro dissolution time

The change in microneedle length with respect to time is summarized in **Table 7-15** as a measure of *in vitro* microneedle dissolution.

Table 7-15. In vitro dissolution profile of various nanocarriers loaded MNP

Time (seconds)	Needle length (μm)*				
	Blank PVA-PVP MNP	VPN UDL MNP	NPT UDL MNP	VPN PNP MNP	NPT PNP MNP
0	1488 ± 51				
30	1176 ± 40	1074 ± 68	1108 ± 41	1143 ± 95	1117 ± 73
60	659 ± 53	598 ± 44	638 ± 56	647 ± 55	625 ± 53
90	249 ± 16	233 ± 16	259 ± 18	266 ± 11	241 ± 13
120	42 ± 4	28 ± 2	34 ± 1	38 ± 1	29 ± 2

* Values represented as Mean ± SD (n=10)

The microneedle length of each MNP was reduced to base within 2 minutes indicating fast dissolving nature of these MNP. No significant difference in dissolution profile of nanocarriers loaded MNP was observed when compared to blank PVA-PVP MNP.

7.3.5.4 Physical stability of nanocarriers in fast dissolving MNP

The transmission electron microscopic images of nanocarriers' dispersions obtained after their MNP dissolution are presented in **Fig. 7-13**. These images showed retention of morphological characteristics by respective nanocarriers indicating their stability within MNP.

Similarly, no significant difference was observed in mean vesicle/particle size as well as entrapment efficiency of nanocarriers' re-dispersion via MNP dissolution (**Table 7-16**) when compared to their initial values.

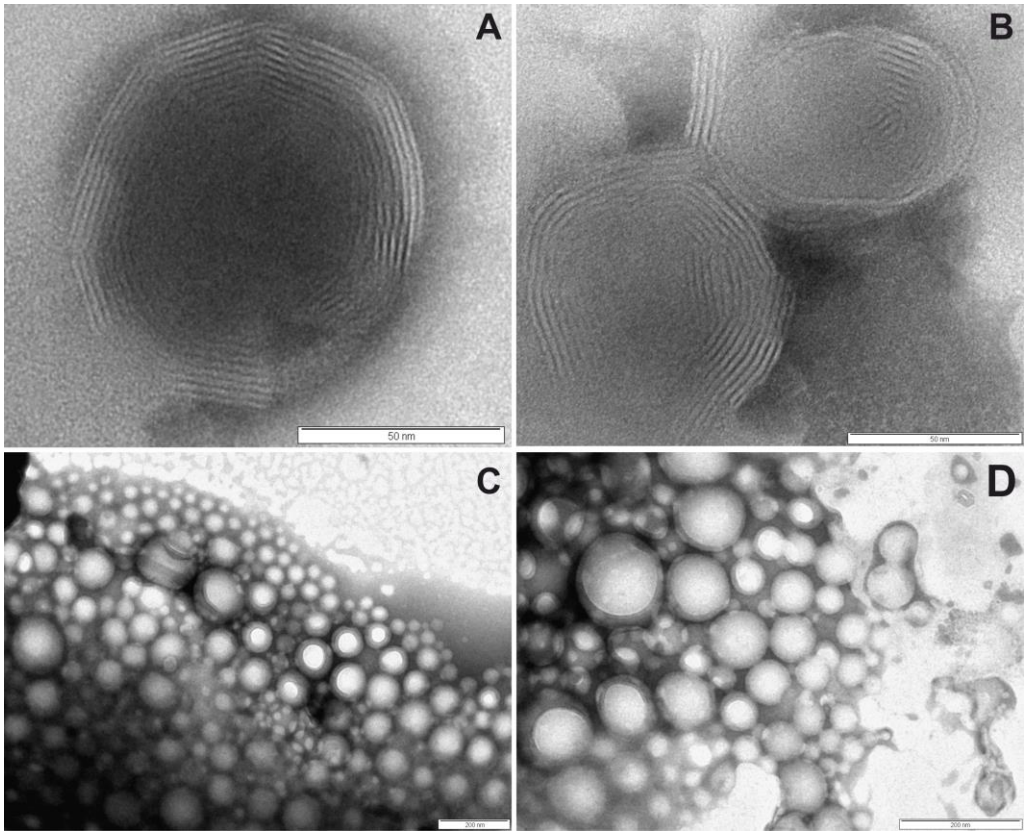

Fig. 7-13. TEM images of A) VPN UDL, B) NPT UDL, C) VPN PNP and D) NPT PNP after re-dispersion from their respective MNP

Table 7-16. Size and entrapment data of nanocarriers' dispersion initially and after re-dispersion via MNP dissolution

Formulations	Vesicle / Particle size (nm)*		Entrapment Efficiency (%)*	
	Initial	Re-dispersion	Initial	Re-dispersion
VPN UDL	75.65 ± 1.66	76.24 ± 2.68	87.44 ± 1.29	86.85 ± 1.57
NPT UDL	67.01 ± 2.79	68.11 ± 3.01	82.65 ± 0.94	82.07 ± 1.25
VPN PNP	104.67 ± 1.73	103.86 ± 3.48	71.59 ± 1.49	71.22 ± 1.84
NPT PNP	80.6 ± 1.55	81.24 ± 2.64	70.73 ± 1.83	70.16 ± 1.88

* Values represented as Mean ± SD (n=3)

7.3.5.5 In vitro drug release

In vitro drug release from nanocarriers loaded MNP was evaluated and the cumulative percent drug release at different time points are summarized in **Table 7-17** as well as illustrated in **Fig. 7-14** below. Release data of all four nanocarriers loaded MNP showed ≥50 % drug release in first 8 hours and > 80 % release in 24 hours. The results showed insignificant decrease in drug release when compared to drug release profile of respective nanocarriers' dispersions (refer chapter 4 and 5). Such

observation indicated that even after increase in viscosity, the drug release from nanocarriers remained rate limiting.

Table 7-17. In vitro release profile of drug from its nanocarriers loaded MNP

Time (h)	Cumulative percent drug released			
	VPN UDL MNP*	VPN PNP MNP*	NPT UDL MNP*	NPT PNP MNP*
0.25	2.84 ± 0.04	3.78 ± 0.07	3.12 ± 0.06	4.58 ± 0.09
0.5	5.27 ± 0.20	7.38 ± 0.22	6.01 ± 0.10	8.04 ± 0.14
1	9.78 ± 0.37	13.97 ± 0.50	10.74 ± 0.21	14.86 ± 0.30
1.5	14.13 ± 0.37	17.89 ± 0.23	13.28 ± 0.25	18.91 ± 0.57
2	17.49 ± 0.70	23.07 ± 0.49	19.17 ± 0.31	21.63 ± 0.36
4	32.28 ± 1.11	33.64 ± 0.86	33.47 ± 0.66	35.14 ± 0.89
6	44.17 ± 1.44	44.37 ± 1.69	44.09 ± 1.41	46.54 ± 1.63
8	50.72 ± 1.09	52.19 ± 1.39	49.93 ± 1.67	51.38 ± 0.92
12	59.93 ± 1.47	60.82 ± 0.81	60.71 ± 0.98	61.73 ± 1.89
24	83.47 ± 2.97	84.96 ± 2.46	83.66 ± 2.56	87.41 ± 3.29

* Result represented as mean ± SD

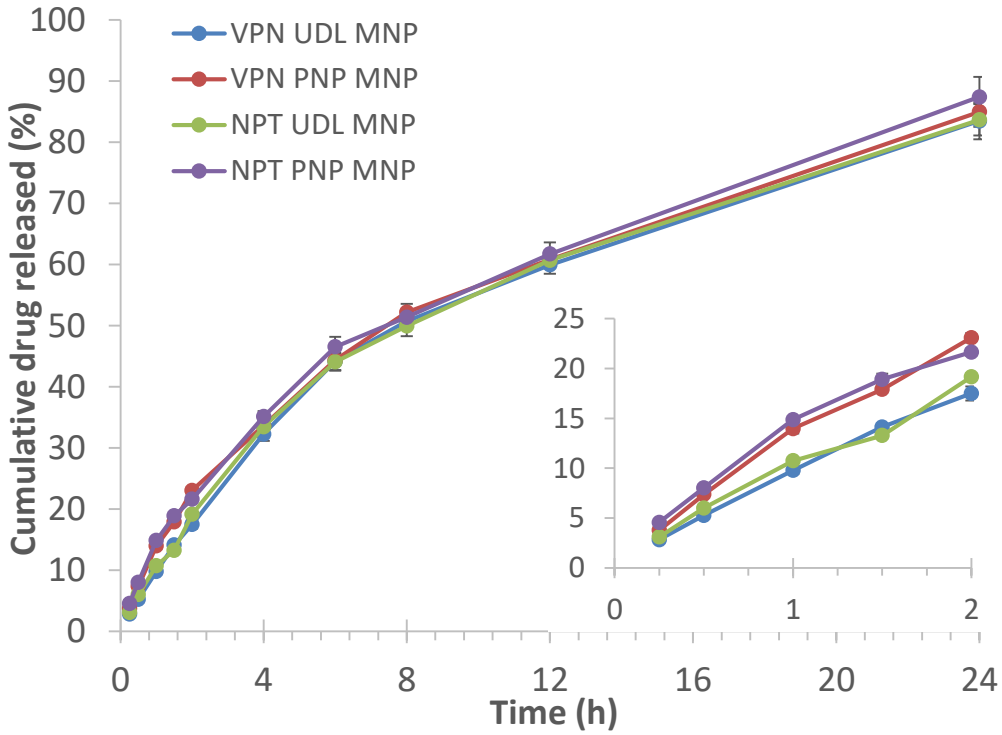

Fig. 7-14. Cumulative percent drug released in vitro versus time curve for all four nanocarriers loaded MNP

The result of various mathematical models, applied to understand the drug release kinetics from nanocarriers loaded MNP, are presented in **Table 7-18**.

Table 7-18. Various mathematical models and their correlation coefficient values

Mathematical models		VPN UDL MNP	VPN PNP MNP	NPT UDL MNP	NPT PNP MNP
Zero order	R^2	0.946	0.949	0.947	0.953
First order		-0.997	-0.997	-0.997	-0.997
Higuchi		0.995	0.997	0.996	0.998
Hixon Crowell		-0.987	-0.989	-0.987	-0.992
Korsmeyer Peppas		0.992	0.990	0.993	0.994
	n	0.81	0.71	0.78	0.67

The R^2 values for Higuchi as well as first order model was found higher suggesting a diffusion controlled system where release rate is dependent on remaining drug concentration within the carrier.

REFERENCES

1. Ita, K., *Dissolving microneedles for transdermal drug delivery: Advances and challenges.* Biomedicine & Pharmacotherapy, 2017. **93**: p. 1116-1127.
2. Kuo, S.-C. and Y. Chou, *A novel polymer microneedle arrays and PDMS micromolding technique.* 淡江理工學刊, 2004. **7**(2): p. 95-98.
3. Lawrence, X.Y., *Pharmaceutical quality by design: product and process development, understanding, and control.* Pharmaceutical research, 2008. **25**(4): p. 781-791.
4. Eriksson, L., et al., *Design of experiments.* Principles and Applications, Learn ways AB, Stockholm, 2000.
5. Lee, J.W., J.H. Park, and M.R. Prausnitz, *Dissolving microneedles for transdermal drug delivery.* Biomaterials, 2008. **29**(13): p. 2113-24.
6. Yan, G., et al., *Evaluation needle length and density of microneedle arrays in the pretreatment of skin for transdermal drug delivery.* Int J Pharm, 2010. **391**(1-2): p. 7-12.
7. Mahvash, M. and P.E. Dupont, *Mechanics of dynamic needle insertion into a biological material.* IEEE Trans Biomed Eng, 2010. **57**(4): p. 934-43.
8. Quinn, H.L., et al., *Design of a Dissolving Microneedle Platform for Transdermal Delivery of a Fixed-Dose Combination of Cardiovascular Drugs.* J Pharm Sci, 2015. **104**(10): p. 3490-500.
9. Akhtar, N., *Microneedles: An innovative approach to transdermal delivery—A review.* Int. J. Pharm. Pharm. Sci, 2014. **6**: p. 18-25.